Commun Nonlinear Sci Numer Simulat 14 (2009) 2670–2676

Contents lists available at ScienceDirect

Commun Nonlinear Sci Numer Simulat

journal homepage: www.elsevier.com/locate/cnsns

A numerical simulation of flow between two rotating coaxial frustum cones

Xiaofei Xu, Lanxi Xu *

Department of Mathematics, Beijing University of Chemical Technology, 100029 Beijing, China

ARTICLE INFO

Article history:
Received 27 September 2007
Received in revised form 11 August 2008
Accepted 23 August 2008
Available online 19 September 2008

PACS:
47.32.–y
47.27.Eq
47.27.Cn

Keywords:
Frustum cone
Reynolds number
Stability
Vortex

ABSTRACT

The behavior of flow between two coaxial frustum cones, with the inner one rotating and the outer stationary, is studied in this paper. It is found that the fluid at the outlet does not flow out directly, but flows up till a certain height. This reflux generates a vortex area with a quite large velocity and pressure magnitude. This reflux area, between $Z/H = 0.05$ and 0.30, has the trend to move up with increasing Reynolds number *Re*. The velocity magnitude is linear in the radial direction if the *Re* is small. This linear relation converts to quasi-quadratic function as the *Re* increasing. If the frustum cone inclination is small, the flow will tend to be unstable with a quite large velocity and pressure magnitude. Finally, a comparison is made with Taylor–Couette flow.

1. Introduction

The flow between two concentric cylinders with the inner one rotating and the outer one stationary, called Taylor–Couette flow (TCF), has been studied by many researchers for decades. With a low rotation rate of the inner cylinder, an analytical solution of the laminar flow with

$$v_r = v_z = 0, \quad v_\theta = \omega_1 r_1 \frac{r_2/r - r/r_2}{r_2/r_1 - r_1/r_2} \tag{1.1}$$

is obtained, where r, θ, z represent the radial, azimuthal, and axial directions of the cylindrical coordinate system, respectively. The angular velocity of the inner cylinder is denoted by ω_1, the inner and outer radii are represented by r_1 and r_2, respectively. The laminar flow becomes unstable when the rotation rate (characterized by Reynolds number *Re*) of inner cylinder reaches a critical value [1]. The flows become turbulent at large Reynolds number. Some results of numerical simulation of turbulent TCF have been reported in [2–5]. In [2–4] different geometric parameters of the TCF apparatus (*Re*, aspect ratio and radius ratio) are taken for studies. It is concluded that there is no unique Reynolds number for the onset of turbulent flow. However, the results show that once the Reynolds number is of the order of 1000 or more, transition to turbulent flow generally occurs.

In this paper we consider a configuration of two concentric frustum cones with the inner frustum rotating and outer fixed (see Fig. 1). A viscous incompressible fluid is contained between the two concentric frustum cones. The property of flow between two coaxial frustum cones (FCF) is quite different from TCF. In this case, it is impossible to find a solution of the form Eq. (1.1). In fact it is to verify that this form of solution does not exist, this is done in another work.

* Corresponding author.
E-mail address: xulx@mail.buct.edu.cn (L. Xu).

1007-5704/$ - see front matter © 2008 Published by Elsevier B.V.
doi:10.1016/j.cnsns.2008.08.019

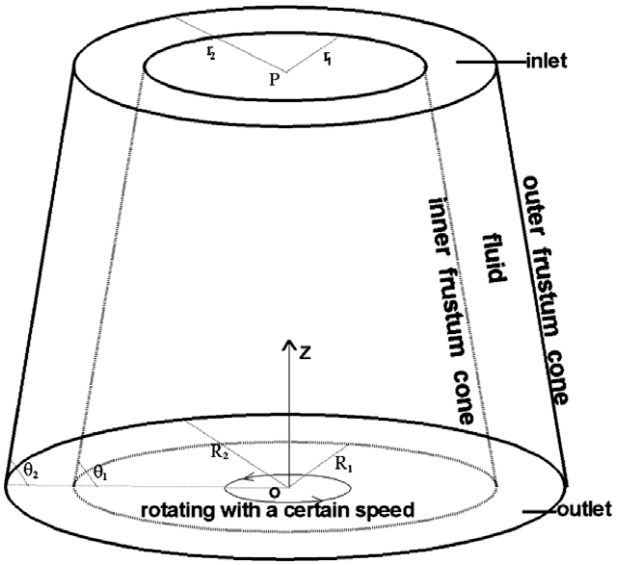

Fig. 1. Sketch of the geometry of the coaxial frustum cones.

Modular design of nano-particle allows for a broad range of applications, such as catalyzing in industrial preparation, purifying in waster treatment and converting photoelectric in solar cell. Many of these applications rely on the fact that an efficient treatment is affected by the particle size. A uniform and suitable particle size would lead a good treating result. In an experiment [6] carried out by a chemist in our university (who used frustum of height 17 mm, outer frustum radii 25 mm for bottom, 20.4 mm for top, $\theta_1 = \theta_2 = 70^\circ$ and the gap width can be adjusted in the range 0.1–0.5 mm), it is found that the diameter of the nano-particle, such as TiO_2, will decrease when it flows out the annular gap. It seems that the nano-particle is ground down in the apparatus. The particle flow out the annular has a uniform size and good appearance. It is also found that the grind strength is proportional to the rotating speed. The higher the rotating speed, the smaller the particle is. It seems that the particle size could be controlled by the rotating speed.

The frusta are not transparent, one cannot observe the real flow. Furthermore, the shape also makes the measurement difficult. In order to study the causes of this effect, we have used numerical techniques here they do not suffer from these limitations. Our primary interest is the numerical simulation of the velocity and pressure magnitude, as well as their dependance on the geometric parameters of the frustum. So far we haven't seen any papers dealing with this problem.

2. Mathematical formulation

The governing equations of the fluid in Fig. 1 are Navier–Stokes equations:

$$\nabla \cdot \boldsymbol{u} = 0 \tag{2.1}$$

$$\partial_t \boldsymbol{u} = \nu \Delta \boldsymbol{u} - \frac{1}{\rho} \nabla p - \boldsymbol{u} \cdot \nabla \boldsymbol{u} \tag{2.2}$$

where $\boldsymbol{u}$, ρ, p and ν denote velocity, density, pressure, and kinematic viscosity of the fluid, respectively. The boundary condition is given by

$$\boldsymbol{u}|_{\sum_i} = \boldsymbol{u}_0 \tag{2.3}$$

$$\omega|_{\sum_1} = \omega_1, \quad \omega|_{\sum_2} = 0 \tag{2.4}$$

where $\sum_i$, $\sum_1$, $\sum_2$ denote the inlet plane, inner and outer frustum, respectively; ω is the angular velocity of the frustum. At the outlet, we assume a zero normal gradient for all the flow variables except the pressure. At $t = 0$ s, the fluid is assumed to be at rest. We set Cartesian coordinate system as shown in Fig. 1. All our results are described in terms of these non-dimensional parameters:

Reynolds number: $Re = \omega_1 L_1 (L_2 - L_1)/\nu$,
Aspect ratio: $\alpha = H/(L_2 - L_1)$,
The ratio of inner to out averaged frustum radius: $\beta = L_1/L_2$,
Angle ratio: $\delta = \theta_1/\theta_2$.

Here, r_1, R_1 (r_2,R_2) denote radius of the top and bottom surface of inner (outer) frustum, respectively; $L_1 = (r_1 + R_1)/2$($L_2 = (r_2 + R_2)/2$) is the average radius of the inner (outer) frustum; H is frustum height, ω_1 is angular velocity of the inner frustum, v is kinematic viscosity of fluid; θ_1 (θ_2) is inner (outer) frustum's inclination.

Remark

(1) All the cases considered in this paper, the inlet's velocity u_0 is assumed to be zero.
(2) All the cases considered in this paper, the angle ratio equals to one, i.e. the inner and outer frustum are in parallel.

3. Outline of the numerical method

The non-linear and time dependent Eqs. (2.1) and (2.2) together with the boundary condition Eqs. (2.3) and (2.4) are integrated numerically using the finite volumes method. For the convection terms in Eq. (2.2), a second-order upwind scheme is used to interpolate the face values of the various quantities from the cell centre values. Central difference quotient is used for the diffusion terms which are always second-order accurate. The temporal discretization involves integrating all the terms in the differential equations with a time step Δt. The integration of the transient terms is implicit by using a second-order formulation. The PISO algorithm is used to link pressure and velocity. The discretized equations are then solved sequentially by using a segregated solver. Convergence is obtained when the residual fall below 10^{-4} for the pressure and the three velocity components.

The grid used for the numerical simulations consists of tetrahedral element. Unsteady flow at high Re values results in steep velocity and pressure gradients in the fluid interior, which requires a finer grid in the radial direction. The averaged gap width $L_2 - L_1$ also determines the grid spacing, for narrow gap need a much finer grid. In order to improve the accuracy and the convergence rate, a coarse correction technique is used. In this technique, three grid levels (adjacent tetrahedral spacing: 0.1, 0.05, and 0.025), which are refined sequentially by slicing it in half in spatial dimensions, are employed. The solution obtained using a coarser grid is interpolated to initialize the solution on the finer grid. It is worth mentioning that the fourth grid level refinement leads to insignificant changes in the obtained solution. To determine the time step for our simulation, we test several steps (Δ = 0.1, 0.05, and 0.01). The residual curve for every testing which reflects the quality of numerical solution, are compared for their smoothing. Taking the calculation amount into consideration, we choose step 0.05 s to our simulation.

To check the reliability of our numerical simulation, we first simulate stable TCF which is a special case of FCF and $\theta_1 = \theta_2 = \frac{\pi}{2}$ has an analytical solution Eq. (1.1). And so we could compare numerical solution to the analytical one. It should be mentioned that Eq. (1.1) is the solution for infinitely long cylinders where endwall effects are ignored. However, the height of checking cylinder is finite (α = 400) for the purpose of unifying the simulation results of frustum and cylinder. The numerical and analytical solution is compared in Fig. 2. They are found to be in approximately agreement. The endwall effect, as described above, may have increased the error shown in Fig. 2.

The maximum value of the error bar is calculated from the standard deviation of all the data. All the codes used in this work are programmed by Fluent.

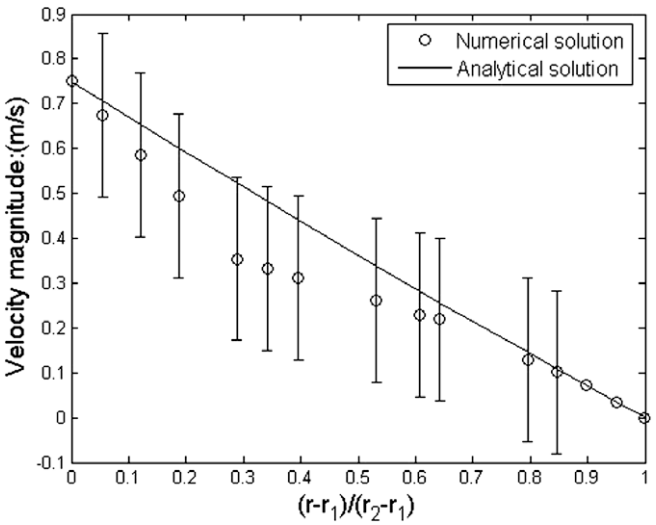

Fig. 2. Numerical solution compared to analytical one for stable TCF in the case of α = 400, β = 0.88, δ = 1, Re = 7.5e + 02.

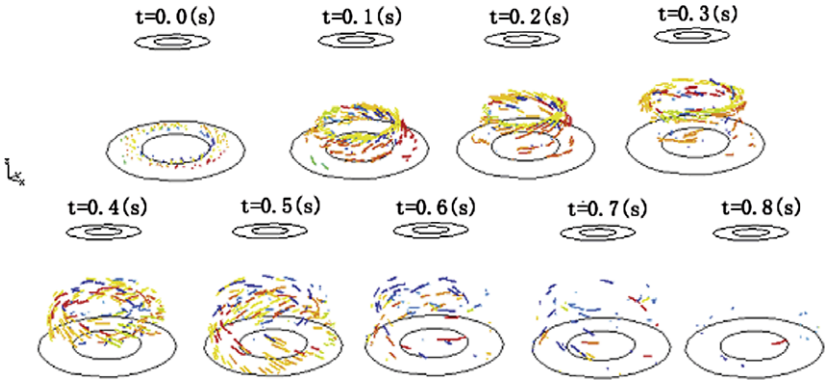

Fig. 3. Streamline evolution nearby outlet for the case of $\alpha = 29.12$, $\beta = 0.88$, $\delta = 1$, $Re = 6.0e + 05$.

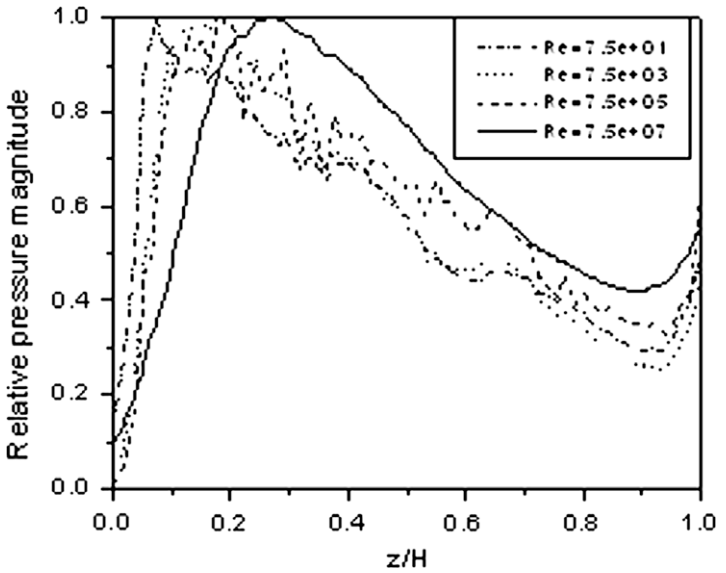

Fig. 4. Relative pressure profiles along Z-direction for the case of $\alpha = 11.36$, $\beta = 0.88$, $\delta = 1$.

4. Results and discussion

4.1. Flow property nearby the outlet

Results of our simulation show that the flow nearby outlet is unstable if Reynolds number exceeds a certain value. This critical value (CV) is determined by the geometry parameters of the frustum. By observing the streamline evolution (Fig. 3), we find that fluid nearby the outlet, not flow out directly, but flow up till a certain height. Staying a relative long time at that special height, this upward flow then flows out the frustum along the outer frustum edge. The duration of this periodic reflux is dependent on Reynolds number and velocity of inlet. As Reynolds number increases, the duration increases and the reflux region (RR) moves upward. The greater the inlet's velocity magnitude, the shorter the duration would be.

Table 1
RR for various Re in the case of $\alpha = 11.36$, $\beta = 0.88$, $\delta = 1$

Reynolds number (Re)	Reflux region Z/H
7.5E + 01	0.06–0.23
7.5E + 03	0.10–0.20
7.5E + 05	0.12–0.23
7.5E + 07	0.21–0.30

4.2. Flow property along axial direction

To study the flow property along axial direction, we conduct several simulations at different Reynolds number in case $\alpha = 11.36$. The relative pressure profiles along axial direction for various values of *Re* are shown in Fig. 4. The data is treated in dimensionless form:

$$p_i = p_i / \max_i(p_i)$$

for the purpose of comparing. With the effect of reflux discussed above, velocity and pressure magnitude reach its maximum in RR along *Z-direction*. This is different from TCF, for the variables of stable TCF are only changing in radial direction.

We regard RR as a region in FCF where velocity or pressure magnitude exceed 90% of their maximum. By observing Fig. 4, the RR for various *Re* is recorded. As it is shown in Table 1, it follows that RR is moving up with the increasing of Reynolds number.

We find that the velocity and pressure are quite large in RR. Especially for small value of α (e.g. $\alpha \leqslant 4$), which implies that the frustum inclination is very small, these quantities are very large, even for the extremely small rotation rate. Their magnitude order for case $\alpha = 1.6$ and various *Re* is shown in the Table 2.

Fig. 5 depicts the vortexes distribution in radial direction at plane $Z/H = 0.2$. It is axisymmetric about axis *Z*-direction. Fig. 6 displays the top view of pressure contour in the fluid interior. The velocity and pressure magnitude of vortex interior is quite large as discussed above. The pressure difference between the interior and exterior of the vortex can reach 10^8 pa. Thus, that is why the fluid particles are ground down in these vortices as described in introduction. The numerical simulation indicates that the numbers of the vortices are even.

4.3. Flow property along radial direction

As $r_1/r_2 \approx 1$, the analytical solution Eq. (1.1) for stable TCF has the form

$$v_\theta = \left(\frac{r_2^2}{r^2} - 1\right)\frac{\omega_1 r_1^2}{r_2^2 - r_1^2} r \approx \left(\frac{r_2^2}{r_1^2} - 1\right)\frac{\omega_1 r_1^2}{r_2^2 - r_1^2} r$$

Table 2
Velocity and pressure magnitude for various values of *Re* in the case of $\alpha = 1.60$, $\beta = 0.88$, $\delta = 1$

Reynolds number (*Re*)	7.5E + 01	7.5E + 03	7.5E + 05	7.5E + 06	7.5E + 07
Velocity magnitude (m/s)	10^5	10^5	10^5	10^6	10^7
Pressure (pa)	10^{11}	10^{11}	10^{11}	10^{12}	10^{14}

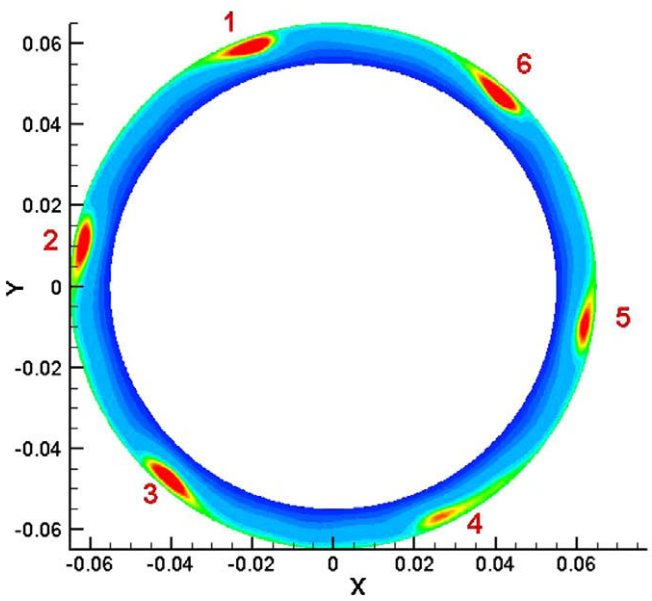

Fig. 5. Streamline distribution in radial direction for the case of $\alpha = 3.68$, $\beta = 0.88$, $\delta = 1$, $Re = 2.75E + 07$. Large and small velocity magnitude is indicated in red and blue, respectively. (For interpretation of the references to color in this figure legend, the reader is referred to the web version of this paper.)

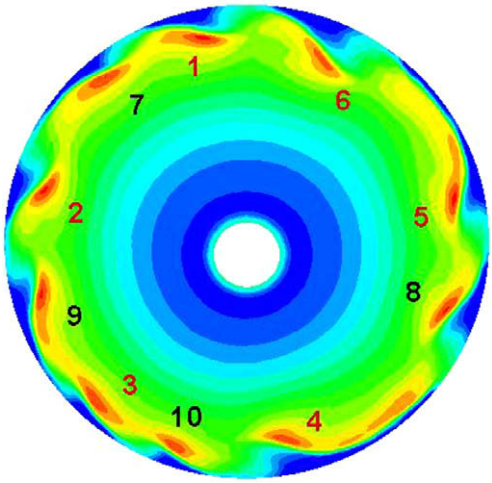

Fig. 6. Top view of pressure contours in the fluid interior for the case of $\alpha = 3.68$, $\beta = 0.88$, $\delta = 1$, $Re = 2.75E+07$. Large and small pressure magnitude is indicated in red and blue, respectively. (For interpretation of the references to color in this figure legend, the reader is referred to the web version of this paper.)

which is linear, with respect to r, approximately. The magnitude reaches its maximum at the inner wall and minimum at the outer wall. In order to study RR's flow property along radial direction, we record the velocity magnitude at plane $Z/H = 0.15$ for various Reynolds numbers. Fig. 7 depicts the average results of our record. The results have been treated in dimensionless form

$$v_i = v_i / \max_i(v_i)$$

for the purpose of comparing. For small Re (about $Re < 7.5$), the same conclusion could be made in FCF. For $7.5 \leqslant Re \leqslant 750$, FCF is in a transition stage whose remarkable phenomenon is that the velocity magnitude nearby inner wall varies small as Reynolds number increases. For $Re \geqslant 750$, the magnitude is a qusi-quadratic function along radial direction and reaches its maximum at point $(r - \rho_1)/(\rho_2 - \rho_1) \approx 0.41$, where $\rho_1(\rho_2)$ denotes the inner (outer) frustum's radius at plane $Z/H = 0.15$.

4.4. Relation of FCF and TCF

We could regard TCF as a limit case of FCF, i.e. inclination of the frustum equals $\pi/2$. In order to study their correlation, we perform simulations for various inclinations with fixing frustum radius. As our pursuit for the cause of particle "grinding

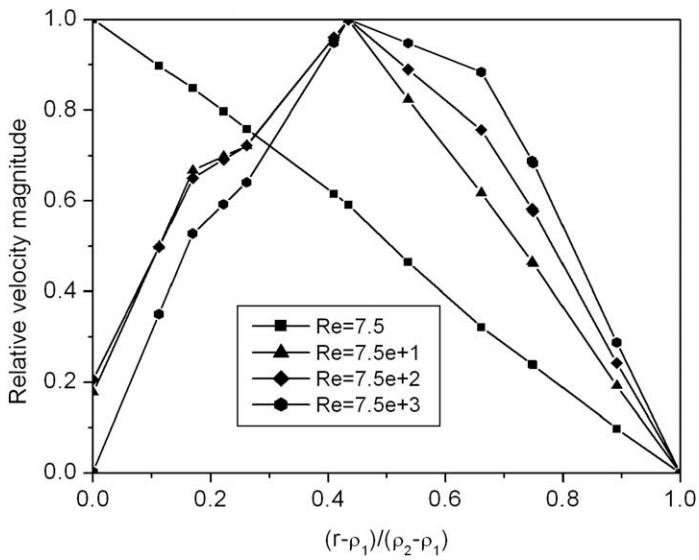

Fig. 7. Relative velocity magnitude profile along radial direction at $Z/H = 0.15$ for the case of $\alpha = 26.08$, $\beta = 0.88$, $\delta = 1$. The data have been treated in dimensionless for the purpose of comparing.

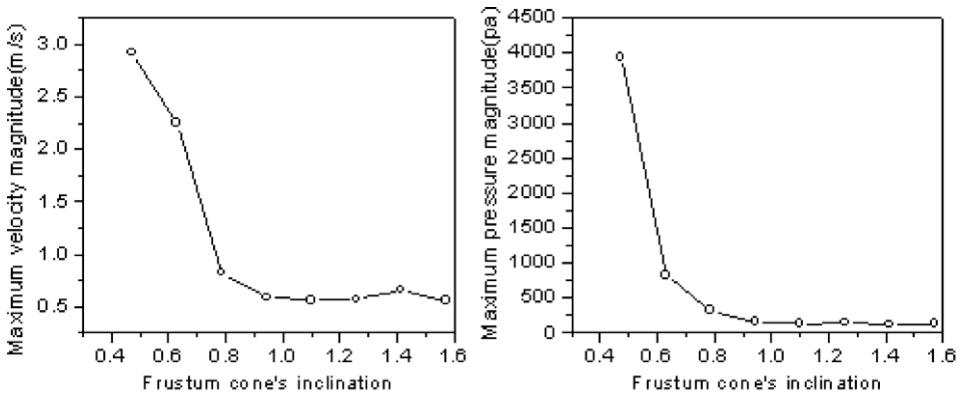

Fig. 8. Maximum of velocity and pressure magnitude varying with frustum inclination for the case of $\beta = 0.88$, $\delta = 1$, $Re = 3.75E+07$.

down" as described in introduction, we hold our attention on the maximum velocity and pressure magnitude in RR. The curves maximum velocity and pressure magnitude in RR as a function of inclinations are sketched in Fig. 8. They are declining curve as the inclination θ increasing. The velocity and pressure magnitude of TCF are the least compared with the other inclination. This implies that TCF is more stable than FCF, i.e. CV of TCF is larger than that of FCF. And it also follows that the smaller the inclination is, the more unstable the flow and the smaller its CV would be. Actually, as $\theta \to \pi/20$, FCF become so turbulent that it cannot be computed effectively by the same model as described in Section 3. It is worth mentioning that there is a critical point θ_0 (about $\pi/4$) for these curves in Fig. 8. The curve is quite flat for $\theta > \theta_0$ and very steep for $\theta < \theta_0$.

5. Conclusions

The present numerical simulation is concerned with behavior of the flow between two rotating coaxial frustum cones (FCF). The fluid contained between the two frusta is incompressible. It is found that the fluid at the outlet does not flow out directly, but flows up till a certain height. This reflux generates a vortex area with a quite large velocity and pressure magnitude. This reflux area (RR), between $Z/H = 0.05$ and 0.30, has the trend to move up with the increasing of the Reynolds number. The velocity magnitude is linear in the radial direction if the Reynolds number is small. The linearly relation converts to quasi-quadratic function as the Reynolds number increasing. The smaller the frustum inclination is, the more unstable the flow will be. Thus TCF is more stable than FCF. The critical Reynolds number for the onset of turbulence in TCF is of the order of 1000 which is larger than that of FCF in the same geometric parameters. For example, it is reported in [7] that the onset of turbulence in TCF for $\alpha = 20$, $\beta = 0.88$ is at $Re = 1500$, however, the transition to turbulent flow in FCF with $\alpha = 20$, $\beta = 0.88$, and $\delta = 1$ occurs at about $Re = 820$.

It is necessary to control the rotation rate in a certain range, for the fluid will not flow out from below if rotation rate is very large. The results of research for this problem are instructive for the application, and it deserves studying in future. Further researches on the flow property with different gap and angle ratio are also expected.

References

[1] Taylor GI. Stability of a viscous liquid contained between two rotating cylinders. Philos Trans Roy Soc Lond 1923;A223:289–343.
[2] Andereck CD, Liu SS, Swinney HL. Flow regimes in a circular Couette system with independently rotating cylinders. J Fluid Mech 1984;164:155–83.
[3] Smith GP, Townsend AA. Turbulent Couette flow between concentric cylinders at large Taylor numbers. J Fluid Mech 1982;123:187–217.
[4] Koschmieder EL. Wavelength measurements in turbulent Taylor vortex flow. J Fluid Mech 1979;93:515–27.
[5] Bilson M, Bremhorst K. Direct numerical simulation of turbulent Taylor–Couette flow. J Fluid Mech 2007;579:227–70. 515–27.
[6] Guo SC, Evans DG, Li DQ. Preparation of Cl pigment 52: 1 anion-pillared layered double hydroxide and the thermo- and photo-stability of the resulting intercalated material. J Phys Chem Solid 2006;6(5):1002–6.
[7] Yuu S, Umekage T. Direct numerical simulation of three-dimensional Navier–Stokes equations for turbulent circular Couette flows ($Re = 1500$) and experimental verification. Kagaku Kogaku Ronbunshu 1995;21(5):886–95 [in Japanese].